Supplementary Information

The Measurement of Relaxation Rates of Degenerate ^{1}H Transitions in Methyl Groups of Proteins Using Acute Angle Radiofrequency Pulses

Vitali Tugarinov* and G. Marius Clore*

Laboratory of Chemical Physics, National Institute of Diabetes and Digestive and Kidney Diseases, National Institutes of Health, Bethesda, MD 20892-0520, USA

Derivation of the values of coefficients *a* and *b* in Eq. (4).

The density matrix ρ describing the state of methyl ^{1}H magnetization after the first ^{1}H 90º pulse in the pulse scheme of Fig. 2A (main text) can be separated into two parts corresponding to the I = 3/2 ($\rho^{3/2}$) and I = 1/2 ($\rho_S^{1/2}$) manifolds (see Fig. 1, main text). These two parts evolve independently of each other under the effect of an RF field, and can be coupled only through relaxation. $\rho^{3/2}$ can be further decomposed into the sum of fast-relaxing (outer) components and a slow-relaxing (inner) component, $\rho^{3/2} = \rho_S^{3/2} + \rho_F^{3/2}$. Here, without loss of generality, we describe the evolution of these matrices under the effect of RF pulses assuming that the first ^{1}H 90º pulse is applied with phase y (ϕ1 in the pulse scheme of Fig. 2A is then shifted by 90º with respect to ϕ1 in the main text). The explicit forms of these density matrices in the basis set of Fig. 1 after the application of a 90º ^1H_y pulse are given by,

$$\rho_S^{3/2} = \begin{bmatrix} 0 & 0 & 0 & 0 \\ 0 & 0 & 1 & 0 \\ 0 & 1 & 0 & 0 \\ 0 & 0 & 0 & 0 \end{bmatrix};\ \rho_S^{1/2} = \frac{1}{2}\begin{bmatrix} 0 & 1 & 0 & 0 \\ 1 & 0 & 0 & 0 \\ 0 & 0 & 0 & 1 \\ 0 & 0 & 1 & 0 \end{bmatrix};\ \rho_F^{3/2} = \begin{bmatrix} 0 & \sqrt{3}/2 & 0 & 0 \\ \sqrt{3}/2 & 0 & 0 & 0 \\ 0 & 0 & 0 & \sqrt{3}/2 \\ 0 & 0 & \sqrt{3}/2 & 0 \end{bmatrix} \quad \text{(S1)}$$

Following the relaxation delay T, each of the density matrices in Eqs. (S1) transform under the effect of a ^{1}H RF pulse applied with flip-angle β according to the solution of the Liouville-von-Neumann equation,

$$\rho(\beta) = e^{-i\beta I_{x,y}}\rho e^{i\beta I_{x,y}} \quad \text{(S2)}$$

where the operators of a ^{1}H pulse applied with phases x and y are defined as,

$$I_x^{3/2} = \begin{bmatrix} 0 & \sqrt{3}/2 & 0 & 0 \\ \sqrt{3}/2 & 0 & 1 & 0 \\ 0 & 1 & 0 & \sqrt{3}/2 \\ 0 & 0 & \sqrt{3}/2 & 0 \end{bmatrix};\ I_y^{3/2} = i\begin{bmatrix} 0 & -\sqrt{3}/2 & 0 & 0 \\ \sqrt{3}/2 & 0 & -1 & 0 \\ 0 & 1 & 0 & -\sqrt{3}/2 \\ 0 & 0 & \sqrt{3}/2 & 0 \end{bmatrix} \quad \text{(S3.1)}$$

for the I = 3/2 manifold, and

$$I_x^{1/2} = \begin{bmatrix} 0 & 1/2 & 0 & 0 \\ 1/2 & 0 & 0 & 0 \\ 0 & 0 & 0 & 1/2 \\ 0 & 0 & 1/2 & 0 \end{bmatrix}; \quad I_y^{1/2} = i\begin{bmatrix} 0 & -1/2 & 0 & 0 \\ 1/2 & 0 & 0 & 0 \\ 0 & 0 & 0 & -1/2 \\ 0 & 0 & 1/2 & 0 \end{bmatrix} \tag{S3.2}$$

for the two $I = 1/2$ manifolds, operating on the column-vectors of eigenfunctions $[|1\rangle, |2\rangle, |3\rangle, |4\rangle]^T$ and $[|5\rangle, |6\rangle, |7\rangle, |8\rangle]^T$, respectively, where the eigenfunctions are defined in the energy level diagram of Fig. 1, and superscript 'T' denotes transposition.

Explicit forms of $\rho(\beta)$ in Eq. (S2) can be found by 'direct exponentiation' techniques as described in detail in our previous publications [1,2]. We obtain that $\rho_S^{3/2}$ and $\rho_F^{3/2}$ transform under the effect of a ^{1}H β pulse phase-cycled as $\pm x$ (*i.e.* applied with the phase collinear with that of ^{1}H magnetization) with retention of the receiver phase, as follows,

$$\rho_S^{3/2} \xrightarrow{\beta(\pm I_x)} \frac{1}{8}\begin{bmatrix} 0 & \sqrt{3}(1-\cos 2\beta) & 0 & 3(1-\cos 2\beta) \\ \sqrt{3}(1-\cos 2\beta) & 0 & (5+3\cos 2\beta) & 0 \\ 0 & (5+3\cos 2\beta) & 0 & \sqrt{3}(1-\cos 2\beta) \\ 3(1-\cos 2\beta) & 0 & \sqrt{3}(1-\cos 2\beta) & 0 \end{bmatrix} \tag{S4.1}$$

and

$$\rho_F^{3/2} \xrightarrow{\beta(\pm I_x)} \frac{1}{8}\begin{bmatrix} 0 & \sqrt{3}(3+\cos 2\beta) & 0 & 3(\cos 2\beta-1) \\ \sqrt{3}(3+\cos 2\beta) & 0 & 3(1-\cos 2\beta) & 0 \\ 0 & 3(1-\cos 2\beta) & 0 & \sqrt{3}(3+\cos 2\beta) \\ 3(\cos 2\beta-1) & 0 & \sqrt{3}(3+\cos 2\beta) & 0 \end{bmatrix} \tag{S4.2}$$

where the non-zero elements of the density matrix are listed for a single scan (neglecting addition of the elements resulting from the phase-cycling), and the state of $\rho_S^{1/2}$ is not affected by this pulse. Under the effect of a ^{1}H β pulse phase-cycled as $\pm y$ (*i.e.* applied with the phase orthogonal to that of ^{1}H magnetization), we obtain,

$$\rho_S^{3/2} \xrightarrow{\beta(\pm I_y)} \frac{1}{16}\begin{bmatrix} 0 & 3\sqrt{3}(\cos\beta-\cos 3\beta) & 0 & 3(\cos 3\beta-\cos\beta) \\ 3\sqrt{3}(\cos\beta-\cos 3\beta) & 0 & 4\cos\beta(9\cos^2\beta-5) & 0 \\ 0 & 4\cos\beta(9\cos^2\beta-5) & 0 & 3\sqrt{3}(\cos\beta-\cos 3\beta) \\ 3(\cos 3\beta-\cos\beta) & 0 & 3\sqrt{3}(\cos\beta-\cos 3\beta) & 0 \end{bmatrix} \tag{S5.1}$$

$$\rho_{S}^{1/2} \xrightarrow{\beta(\pm I_y)} \frac{1}{2}\begin{bmatrix} 0 & \cos\beta & 0 & 0 \\ \cos\beta & 0 & 0 & 0 \\ 0 & 0 & 0 & \cos\beta \\ 0 & 0 & \cos\beta & 0 \end{bmatrix} \tag{S5.2}$$

and for the fast-relaxing part,

$$\rho_{F}^{3/2} \xrightarrow{\beta(\pm I_y)} \frac{1}{16}\begin{bmatrix} 0 & \sqrt{3}(5\cos\beta+3\cos 3\beta) & 0 & 3(\cos\beta-\cos 3\beta) \\ \sqrt{3}(5\cos\beta+3\cos 3\beta) & 0 & 36\cos\beta(1-\cos^2\beta) & 0 \\ 0 & 36\cos\beta(1-\cos^2\beta) & 0 & \sqrt{3}(5\cos\beta+3\cos 3\beta) \\ 3(\cos\beta-\cos 3\beta) & 0 & \sqrt{3}(5\cos\beta+3\cos 3\beta) & 0 \end{bmatrix} \tag{S5.3}$$

Considering that only slow-relaxing (inner) ^{1}H transitions are selected for observation by the pulse-scheme of Fig. 2A, *i.e.* along with $\rho_{S}^{1/2}$, only the elements [2,3] or [3,2], *italicized* in the matrices in Eqs. (S4) and Eqs. (S5.1, S5.3), contribute to detectable magnetization at the end of the experiment, we can calculate for phase *x* of the β pulse the parts of the observable signal derived from the slow- and fast-relaxing magnetization during *T* (coefficients *a* and *b*, respectively) as, $a = 2\,\rho_{S}^{3/2}(\beta)[2,3] + 1 = (3/4)(3 + \cos 2\beta)$, and $b = 2\,\rho_{F}^{3/2}(\beta)[2,3] = (3/4)(1 - \cos 2\beta)$, where the elements of ρ are taken from Eqs. (S4). The corresponding expressions for phase *y* of the β pulse, are: $a = 2\,\rho_{S}^{3/2}(\beta)[2,3] + \cos\beta = (3/2)\cos\beta(3\cos^2\beta - 1)$, and $b = 2\,\rho_{F}^{3/2}(\beta)[2,3] = (9/2)\cos\beta(1 - \cos^2\beta)$, where the elements of ρ are taken from Eqs. (S5.1) and (S5.3). These expressions for *a* and *b* are the same as in the main text to within a multiplication factor.

Identical results can be obtained using an irreducible tensor-based approach described for magnetically equivalent protons in methyl groups by Ernst, Bodenhausen and co-workers [3,4,5]. Below, we briefly describe how the irreducible tensor formalism can be adapted for derivation of the matrix elements of $\rho^{3/2}(\beta)$. For the sake of brevity, we focus only on the slow-relaxing part of the density matrix of the $I = 3/2$ manifold, $\rho^{3/2}$ (*i.e.* the elements [2,3] and [3,2] of $\rho^{3/2}$ that are effectively observed at the end of the experiment in Fig. 2A). The rest of the derivation of coefficients *a* and *b* in Eq. (4) of the main text remains the same as described above.

After the first ^{1}H 90^o excitation pulse with phase *y*, the state of the density matrix ρ can be expressed as the following linear combination of irreducible tensor operators of rank *l* and coherence *p* ($T_{l,p}$) for spin 3/2 [3],

$$\rho = \sqrt{\frac{5}{2}}\left(T_{1,-1} - T_{1,1}\right) \tag{S6}$$

where the same matrix forms of the tensors $T_{l,p}$ is used as in ref. [3],

$$T_{1,-1} = \frac{1}{\sqrt{10}}\begin{pmatrix} 0 & 0 & 0 & 0 \\ \sqrt{3} & 0 & 0 & 0 \\ 0 & 2 & 0 & 0 \\ 0 & 0 & \sqrt{3} & 0 \end{pmatrix};\ T_{1,1} = \frac{1}{\sqrt{10}}\begin{pmatrix} 0 & -\sqrt{3} & 0 & 0 \\ 0 & 0 & -2 & 0 \\ 0 & 0 & 0 & -\sqrt{3} \\ 0 & 0 & 0 & 0 \end{pmatrix} \tag{S7}$$

To adapt this approach for our purposes, we first decompose the density matrix represented by these operators, onto the fast- and slow-relaxing parts denoted by the subscripts '*F*' and '*S*', respectively, as follows,

$$\begin{aligned} T_{1,-1} &= T_{F,-1} + T_{S,-1} \\ T_{1,1} &= T_{F,1} + T_{S,1} \end{aligned} \tag{S8}$$

where

$$\begin{aligned} T_{F,p} &= \frac{3}{5}T_{1,p} + \frac{\sqrt{6}}{5}T_{3,p} \\ T_{S,p} &= \frac{2}{5}T_{1,p} - \frac{\sqrt{6}}{5}T_{3,p} \end{aligned} \tag{S9}$$

for $p \in \{1, -1\}$, where

$$T_{3,-1} = \frac{1}{\sqrt{5}}\begin{pmatrix} 0 & 0 & 0 & 0 \\ 1 & 0 & 0 & 0 \\ 0 & -\sqrt{3} & 0 & 0 \\ 0 & 0 & 1 & 0 \end{pmatrix};\quad T_{3,1} = \frac{1}{\sqrt{5}}\begin{pmatrix} 0 & -1 & 0 & 0 \\ 0 & 0 & \sqrt{3} & 0 \\ 0 & 0 & 0 & -1 \\ 0 & 0 & 0 & 0 \end{pmatrix} \tag{S10}$$

The fast- and slow-relaxing parts correspond to transitions {|1><2|, |3><4|} (shown in blue) and |2><3| (shown in red), respectively, in the I = 3/2 manifold of the spin energy level diagram in Fig. 1 (main text).

Each individual tensor operator $T_{l,p}$ transforms under the effect of an RF pulse with flip-angle β and phase ϕ according to an irreducible representation of the rotation group [3,5],

$$T_{l,p} \xrightarrow{\beta(-I_x \sin\phi + I_y \cos\phi)} \sum_{p'} T_{l,p'} d^{l}_{p',p}(\beta) e^{-i\Delta p\phi} \tag{S11}$$

where Δp is the change in coherence order (p' - p), and $d^{l}_{p',p}$ are the elements of the reduced Wigner rotation matrices of rank l. Note that phase x in this convention corresponds to ϕ = -π/2, while phase y corresponds to ϕ = 0. For the convenience of the reader, we list the elements of the reduced Wigner rotation matrices for l =1 and 3,

$$\begin{aligned} d^{1}_{0,-1} &= -d^{1}_{0,1} = \left(1/\sqrt{2}\right)\sin(\beta) \\ d^{1}_{1,-1} &= d^{1}_{-1,1} = \sin^2(\beta/2) \\ d^{1}_{1,1} &= d^{1}_{-1,-1} = \cos^2(\beta/2) \end{aligned} \tag{S12.1}$$

and

$$\begin{aligned} d^{3}_{0,1} &= -d^{3}_{0,-1} = \left(\sqrt{3}/4\right)\sin\beta\left(5\cos^2\beta - 1\right) \\ d^{3}_{1,-1} &= d^{3}_{-1,1} = \frac{1}{8}(1-\cos\beta)\left(15\cos^2\beta + 10\cos\beta - 1\right) \\ d^{3}_{1,1} &= d^{3}_{-1,-1} = \frac{1}{8}(1+\cos\beta)\left(15\cos^2\beta - 10\cos\beta - 1\right) \end{aligned} \tag{S12.2}$$

Transforming $T_{S,p}$ and $T_{F,p}$ according to the transformation rule in Eq. (S11) for the pulse with phase ϕ = -π/2 (x) and focusing only on the slow-relaxing ^{1}H transitions of the I = 3/2 manifold (|2><3| or |3><2|; Fig. 1), yields,

$$\sqrt{\frac{5}{2}}(T_{S,-1} - T_{S,1}) \xrightarrow{\beta(I_x)} \frac{1}{8}\left(3\cos 2\beta + 5\right) \tag{S13.1}$$

$$\sqrt{\frac{5}{2}}(T_{F,-1}-T_{F,1}) \xrightarrow{\beta(I_X)} \frac{3}{8}\left(1-\cos 2\beta\right) \tag{S13.2}$$

while for the β pulse applied with $\phi = 0$ (y) we obtain,

$$\sqrt{\frac{5}{2}}(T_{S,-1}-T_{S,1}) \xrightarrow{\beta(I_y)} \frac{1}{4}\cos\beta\left(9\cos^2\beta-5\right) \tag{S14.1}$$

$$\sqrt{\frac{5}{2}}(T_{F,-1}-T_{F,1}) \xrightarrow{\beta(I_y)} \frac{9}{4}\cos\beta\left(1-\cos^2\beta\right) \tag{S14.2}$$

The resulting elements of the density matrix $\rho(\beta)$ in Eqs. (S13) and (S14) are identical to the (italicized) elements [2,3] and [3,2] of the corresponding matrices $\rho^{3/2}$ in Eqs. (S4) and (S5.1, S5.3), respectively. It is worth noting that owing to the uniform transformation rule for each tensor operator in Eq. (S11), as long as the elements of the density matrix of interest (the detectable parts of the magnetization) are isolated and focused on, the irreducible tensor-based approach substantially simplifies the calculation of the elements of $\rho(\beta)$.

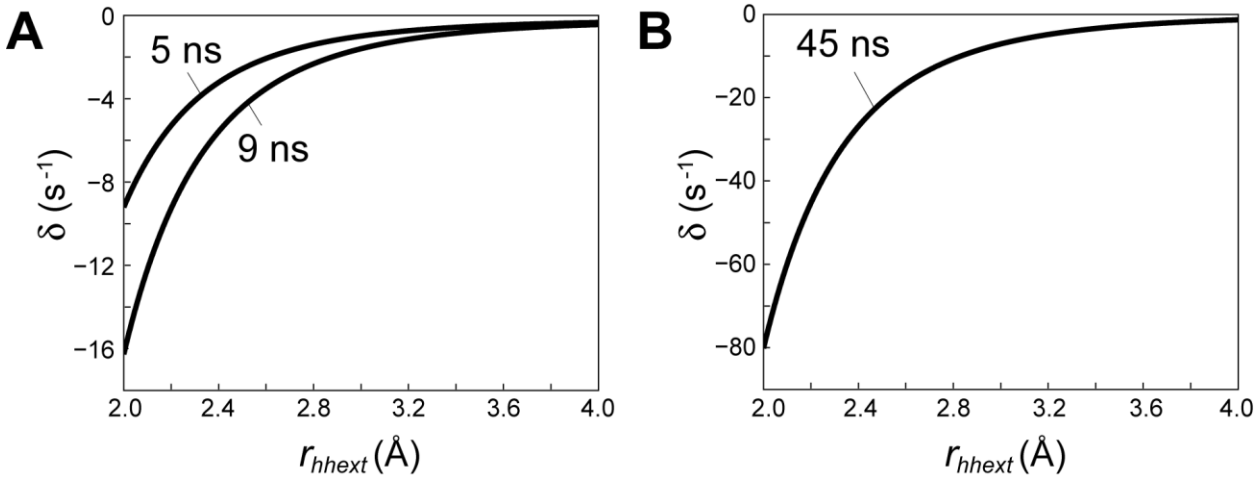

Figure S1. Plots showing the values of cross-relaxation rates δ (s^{-1}) as a function of the distance to a single external proton spin, r_{hhext} (Å) for global molecular correlation times (**A**) τ_C = 5 and 9 ns, and (**B**) τ_C = 45 ns. In the limit where $r_{hhext} \rightarrow \infty$ (in the absence of spin-flips), δ asymptotically approaches values of -0.21, -0.19, and -0.07 s^{-1} for τ_C = 5 and 9 ns (A) and τ_C = 45 ns (B), respectively. Calculations were performed using the basis set of ^{1}H transitions and the form of the spectral density function described in the Supplementary Information of ref. [6], along with the same set of methyl geometry parameters, namely, $\theta_{axis,CH} = 110.4^o$, r_{CH} = 1.117 Å, and $r_{HH} = \sqrt{3}\sin(\theta_{axis,CH})r_{CH}$ = 1.813 Å. The amplitude of methyl axis motions, S^2_{axis}, was set to 0.6, and the correlation time for fast, local motions, τ_f, to 40 ps.

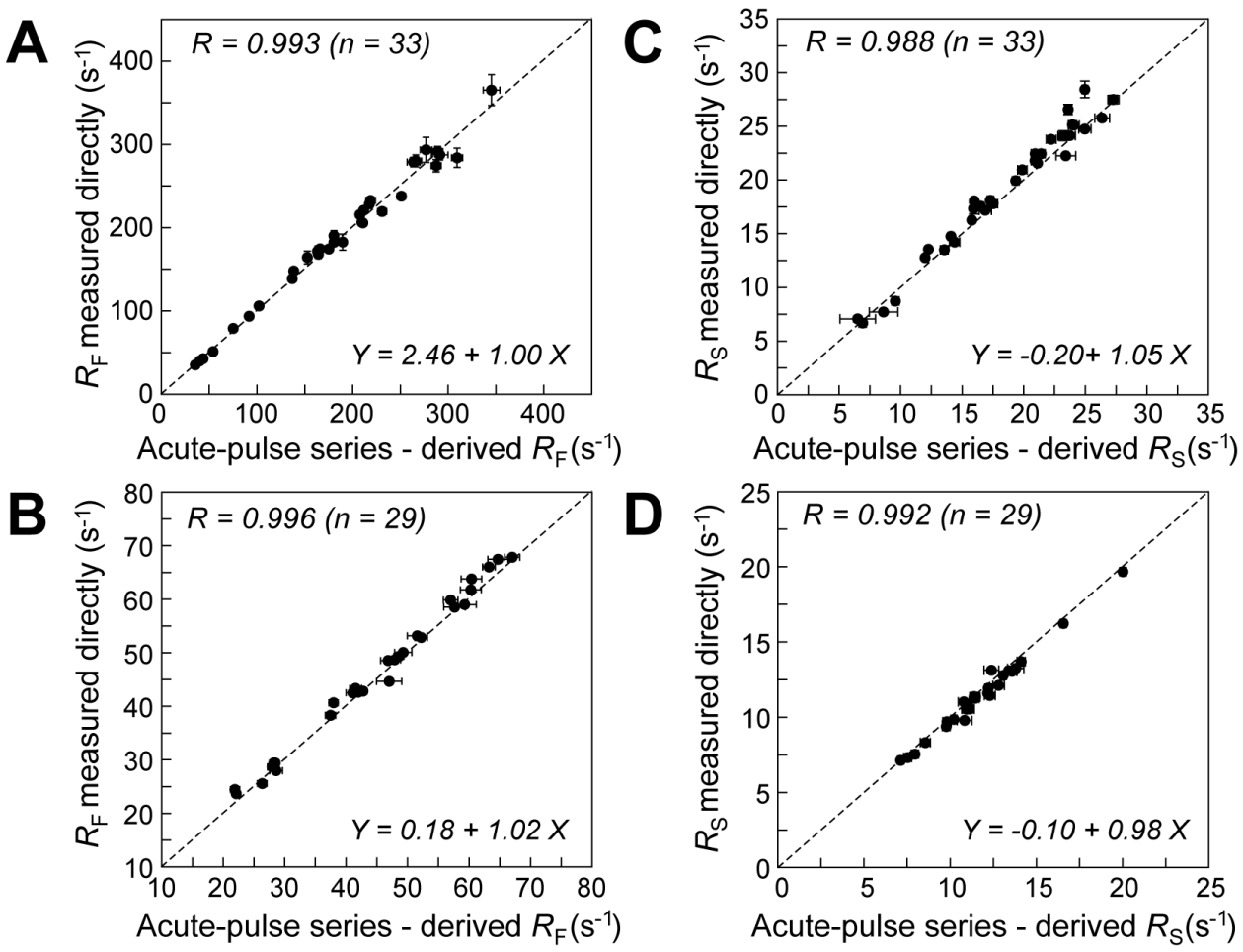

Figure S2. Correlation plots comparing the rates R_F (s^{-1}) obtained from acute-pulse R_2 series (*x*-axes) and 'direct' measurements (*y*-axes) for methyls of (**A**) Ile$^{\delta 1}$-{$^{13}CH_3$}-labeled MSG, and (**B**) ILV-{$^{13}CH_3$}-labeled ubiquitin. Correlation plots comparing the rates R_S (s^{-1}) obtained from acute-pulse R_2 series (*x*-axes) and 'direct' measurements (*y*-axes) for methyls of (**C**) MSG, and (**D**) ubiquitin. Linear correlation coefficients *R* and the parameters of linear regression for the total number of *n* methyl sites are indicated on each plot. Dashed lines are drawn at $y = x$. All NMR data were collected at 600 MHz.

Materials and Methods

NMR Samples. The {U-[^{15}N,^{2}H]; Ile$^{\delta1}$-[^{13}CH$_3$]; Leu,Val-[^{13}CH$_3$,^{12}CD$_3$]}-labeled sample of ubiquitin was prepared as described previously [7] using appropriate α-keto-acid precursors. The concentration of ubiquitin was 1.3 mM in a buffer containing 99.9% D_2O, 20 mM sodium phosphate (pH 6.5; uncorrected) and 50 mM NaCl. The sample of {U-[^{15}N,^{2}H]; Ileδ1-[^{13}CH$_3$]}-labeled Malate Synthase G (MSG) was prepared as described previously [8] and dissolved in a buffer containing 99.9% D_2O, 25 mM sodium phosphate (pH 7.0; uncorrected) and 5 mM $MgCl_2$.

NMR Spectroscopy. All spectra were recorded on a 600 MHz, AVANCE HD Bruker spectrometer equipped with a triple-axis (*x*, *y*, *z*) gradient cryogenic probe, at 10º and 37 ºC for Ile$^{\delta1}$-{^{13}CH$_3$}-MSG and ILV-{^{13}CH$_3$}-ubiquitin, respectively. The spectra were processed and analyzed using the NMRPipe/NMRDraw programs and associated software [9]. Each of the 2D spectra acquired with the pulse-scheme in Fig. 2A (main text) comprised [64, 512] complex points in the [^{13}C(t_1), ^{1}H(t_2)] dimensions translating to acquisition times of [21 ms, 64 ms] and [42 ms, 64 ms] for ubiquitin and MSG, respectively. Typically, 24 scans per FID with an inter-scan recovery delay of 1.6 sec were used leading to net acquisition times of ~1.5 hr. per 2D spectrum.

The experiments in Fig. 2A were recorded in an interleaved manner as a function of the parametrically varied relaxation delay *T* for each value of the angle β resulting in pseudo-4D sets of data. The following set of delays *T* was used for Ile$^{\delta1}$-{^{13}CH$_3$}-MSG in the experiment recorded with ϕ1 = *y*,-*y*: (1.5, 3.1, 4.3, 6.3, 8.3, 10.3, 12.3, 14.3, 16.3, 18.3, 20.3, 22.3) ms. The sets of *T* values used for ILV-{^{13}CH$_3$}-ubiquitin were (2.1, 10.3, 16.3, 20.3, 24.3, 32.3, 36.3, 40.3, 48.3, 60.3, 70.3, 80.3) ms, and (2.1, 5.1, 8.3, 12.3, 16.3, 20.3, 24.3, 28.3, 32.3, 40.3) ms for the experiments acquired with ϕ1 = *y*,-*y* and ϕ1 = *x*,-*x*, respectively. The sets of (nominal) angles β were: (10º, 30º, 40º, 50º, 65º, 90º) in experiments recorded with ϕ1 = *y*,-*y* (for both proteins) and (41º, 49º) in experiments recorded with ϕ1 = *x*,-*x* (ubiquitin only). ^{1}H pulses are calibrated first in a regular manner on residual water ($^{1}H_2O$) signal. Subsequently, the ^{1}H pulses are 'fine-tuned' on-resonance (placing the carrier on methyl ^{1}H signals). The 'fine-tuning' of the flip-angles β was performed in a pseudo-3D manner using the pulse-scheme in Fig. 2A with ϕ1 = *x*,-*x*, *T* = 0, the gradients g2 and composite ^{13}C pulses omitted (see main text) with parametrically varied angles β. The values of $\beta = \cos^{-1}(I/I_0)$ calculated for all methyl cross-peaks in the 2D spectra were averaged to obtain the 'true' values of the angle, which were subsequently used in data analysis. In practice, thus 'fine-tuned' angles β were within 1-2º of their corresponding nominal values (which are reported in the main text). Specifically, the set of angles β calibrated in this manner for MSG

and ubiquitin in the experiment with $\phi 1 = y,-y$ were: (9.7º, 29.4º, 39.4º, 49.6º, 64.8º, 90.5º) and (10.1º, 30.3º, 40.4º, 50.7º, 66.0º, 91.7º), respectively, while in the experiment with $\phi 1 = x,-x$ (ubiquitin only), the calibrated angles were (41.5º, 49.7º).

The 3Q relaxation-violated coherence transfer ('forbidden') experiments were recorded using the pulse scheme described previously [10] with the following sets of relaxation delays T: (1.5, 2.7, 3.9, 5.1, 6.3, 7.5, 8.7, 9.9, 11.1, 12.3, 13.5, 14.7) ms, and (2.1, 8.3, 12.3, 16.3, 20.3, 24.3, 28.3, 32.3, 36.3, 40.3, 44.3, 48.3) ms for MSG and ubiquitin, respectively.

'Direct' measurements of relaxation rates R_F and R_S (via isolation of the fast- and slow-relaxing components prior to rate measurements) were performed using the pulse schemes described in ref. [6] and ref. [2] for MSG and ubiquitin, respectively. The following sets of relaxation delays T: (1.2, 1.8, 2.6, 3.4, 4.2, 5.0) ms, and (2.1, 8.3, 12.3, 16.3, 20.3, 24.3) ms were used for R_F measurements in MSG and ubiquitin, respectively. The corresponding delays for R_S measurements were set to (1.2, 8.2, 16.2, 24.2, 32.2, 40.2) ms, and (2.1, 20.3, 40.3, 60.3, 80.3, 100.3) ms, respectively.

Data Analysis. All relaxation (R_2) decay series acquired using the pulse scheme in Fig. 2A were fitted simultaneously to Eq. (4), where $F(T)$ and $S(T)$ are given by Eqs. (2), as described in the main text, with appropriate values of coefficients a and b, calculated using the calibrated angles β (see above). To obtain equal quality of the fits for all R_2 decays of the series, we found it advantageous to scale the uncertainties in data points entering the target function by their corresponding normalized intensities. This ensures that the errors in data points of R_2 decays that show more substantial decrease in intensity (for larger angles β in the experiment of Fig. 2A with $\phi 1 = y,-y$; see Figs. 3A, B of the main text) contribute to the total error function on par with R_2 decays with only minor losses in intensities (as is the case for smaller angles β).

The rates R_F and R_S rates in 'direct' measurements were obtained by fitting relaxation decays to a single-exponential function, $I_0\exp(-RT)$, where R is relaxation rate, and I_0, initial intensity. The build-ups of the ratios of signal intensities in all 3Q 'forbidden' data were fitted to Eq. (3) of the main text (C = 3/4), using two variable parameters, η and δ. The uncertainties in experimental intensities (peak heights) were determined from the noise-floor of 2D spectra, while the uncertainties in the values of the optimized parameters, corresponding to confidence intervals of ±1 standard deviation, were established in all cases from the variance-covariance matrix of the nonlinear fit.

Pulse code for experiment in Fig. 2A

```
#include <Avance.incl>
#include <Grad.incl>

define delay TAUB
"TAUB=1.0m - p24 - 2u"

define delay COMPH
"COMPH = p1*0.63662"          ;; p1*2/pi

define delay DGRAD
"DGRAD = p22 + 2u"

"d3=4.0m - p23 - 2u"
"d4=4.0m - p23 - 4u - p8"

"d11=1m"
"d12=1m"

;; define list of pulse-lengths in micro-seconds
define list<pulse> PW_ALPHA={0.9389 2.8167 3.7555 4.6944 6.1028 8.450}

;; define list of relaxation times in seconds
define list<delay> TIME_T2={0.0003 0.0007 0.001 0.0015 0.002 0.0025 0.003 0.0035 0.004 0.0045 0.005 0.0055}

;; initial carbon evolution delay
"d0=in0*0.5 - p8*0.3183 - p1"      ;; p8*1/pi

;; p1@pl1 - hard 1H pulse
;; p2@sp2 – water-selective 1H Eburp-1 pulse, ~ 7ms
;; p8@pl8 - hard 13C pulse
;; pcpd2@pl31 - 13C decoupling

;; l3  - number of real t1 points (TD1/2)
;; l2  - number of T2 relaxation delays (12)
;; l6  - number of beta angles (6)

;; ---------------------- real start here ------------------------

1  ze
2  5u do:f2
3  5u do:f2
4  5u do:f2
5  5u do:f2
6  5u do:f2

;; ---------------- 1H spin-lock between scans -----------

  2u pl9:f1                          ;; ~10-kHz (250u) SLy pulse
  (p9 ph7):f1                        ;; 40-ms spin-lock (SLy) pulse
  2u pl1:f1
```

```
  p21:gp1
  200u
  (p1 ph0):f1
  2u
  p21*0.5:gp1

;; ----------------------------------------------------------------

  1m BLKGRAD
  d1
  1m UNBLKGRAD

  10u pl8:f2
  10u pl0:f1
  (p2:sp2 ph0:r):f1                ;; water-selective Eburp-1 pulse: ~7 ms
  2u
  (p8 ph0):f2
  2u
  p20:gp0
  1m pl1:f1

;; ---------- relaxation period start ----------

   (p1 ph0):f1
   DGRAD

   TIME_T2

   (p8 ph7):f2
   (p8*2 ph0):f2
   (p8 ph7):f2

   2u
   p22:gp2

   TIME_T2

   (p1*2 ph0):f1

   2u
   p22:gp2

   TIME_T2
   COMPH

   (p8 ph7):f2
   (p8*2 ph0):f2
   (p8 ph7):f2

   DGRAD
   TIME_T2
   COMPH
```

```
;; ---------- relaxation period end ----------

   (PW_ALPHA ph1):f1                    ;; beta pulse (variable angle)

   2u
   p23:gp3
   d3

;; ---------- filter fast lines out ----------

   (p8 ph2):f2
   2u
   p24:gp4
   TAUB
   (center (p8*2 ph0):f2 (p1*2 ph0):f1)
   2u
   p24:gp4
   TAUB
   (p8 ph3):f2

;; ********** carbon evolution **********

   d0
   (p1*2 ph0):f1
   d0

;; ********** back to protons **********

   (p8 ph4):f2
   (p1*2 ph0):f1
   2u
   p23:gp3
   d4
   (p8 ph0):f2
   (p8 ph5):f2
   2u pl31:f2

;; ********** acquisition start **********

   go=2 ph31 cpds2:f2
   10u do:f2
   d11 wr #0 if #0 zd

;; ----------------------------------------------------------

   d12 PW_ALPHA.inc
   lo to 3 times l6

   d12 TIME_T2.inc
   lo to 4 times l2

   d12 ip4
   lo to 5 times 2
```

```
   d12 id0
   d12 ip31
   d12 ip31
   lo to 6 times l3


10u do:f2
1m BLKGRAD
exit

;; ---------- phase cycling ----------

ph0=0
ph1=1 3       ;; 0 2 for ‘orthogonal’ expt.
ph2=0 2
ph3=1 1 3 3
ph4=0
ph5=0 0 0 0 2 2 2 2
ph7=1
ph31=0 2 0 2 0 2 0 2
```

Supplementary References

[1] V. Tugarinov, T.K. Karamanos, A. Ceccon, G.M. Clore, Optimized NMR experiments for the isolation of I = 1/2 manifold transitions in methyl groups of proteins, Chemphyschem 21 (2020) 13-19.

[2] V. Tugarinov, T.K. Karamanos, G.M. Clore, Magic-angle-pulse driven separation of degenerate ^{1}H transitions in methyl groups of proteins: application to studies of methyl axis dynamics, Chemphyschem 21 (2020) 1087-1091.

[3] N. Müller, G. Bodenhausen, R.R. Ernst, Relaxation-induced violations of coherence transfer selection rules in nuclear magnetic resonance, J. Magn. Reson. 75 (1987) 297-334.

[4] G. Jaccard, S. Wimperis, G. Bodenhausen, Multiple-quantum NMR spectroscopy of S = 3/2 spins in isotropic phase: A new probe for multiexponential relaxation, J. Chem. Phys. 85 (1986) 6282-6293.

[5] R.R. Ernst, G. Bodenhausen, A. Wokaun, Principles of nuclear magnetic resonance in one and two dimensions, Oxford University Press, Oxford, 1987.

[6] V. Tugarinov, L.E. Kay, Separating degenerate ^{1}H transitions in methyl group probes for single-quantum ^{1}H-CPMG relaxation dispersion NMR spectroscopy, J. Am. Chem. Soc. 129 (2007) 9514-9521.

[7] A. Ceccon, V. Tugarinov, A. Bax, G.M. Clore, Global dynamics and exchange kinetics of a protein on the surface of nanoparticles revealed by relaxation-based solution NMR spectroscopy, J. Am. Chem. Soc. 138 (2016) 5789-5792.

[8] V. Tugarinov, R. Muhandiram, A. Ayed, L.E. Kay, Four-dimensional NMR spectroscopy of a 723-residue protein: chemical shift assignments and secondary structure of Malate Synthase G, J. Am. Chem. Soc. 124 (2002) 10025-10035.

[9] F. Delaglio, S. Grzesiek, G.W. Vuister, G. Zhu, J. Pfeifer, A. Bax, NMRPipe: a multidimensional spectral processing system based on UNIX pipes, J. Biomol. NMR 6 (1995) 277-293.

[10] H. Sun, L.E. Kay, V. Tugarinov, An optimized relaxation-based coherence transfer NMR experiment for the measurement of side-chain order in methyl-protonated, highly deuterated proteins, J. Phys. Chem. B 115 (2011) 14878-14884.